

Optimal Feedback Rate Selection for Energy Harvesting with Distributed Transmit Beamforming

Rui Wang and D. Richard Brown III
Dept. of Electrical and Computer Eng.
Worcester Polytechnic Institute
100 Institute Rd, Worcester, MA 01609
Email: {rwang, drb}@wpi.edu

Abstract—This paper considers wireless power transfer with feedback-based distributed transmit beamforming in a narrow-band setting where all nodes have independent local oscillators with stochastic dynamics. The receive node provides periodic feedback to the transmit nodes to facilitate efficient wireless power transfer. The optimal feedback rate to maximize the amount of energy harvested by the receive node per unit of time is analyzed and a method to numerically calculate the optimal feedback rate is provided. The results demonstrate that the efficiency of wireless power transfer can be significantly improved with feedback-based distributed transmit beamforming and feedback rate optimization.

Index Terms—wireless power transfer, distributed transmit beamforming, energy harvesting, oscillator dynamics, synchronization, channel state feedback

I. INTRODUCTION

Wireless power transfer (WPT) using radio frequency signals is a technique that facilitates the transmission of electrical power from a source to a receiver over a wireless link in cases where interconnecting wires are inconvenient, hazardous, or not possible [1]–[4]. While prior work has focused primarily on point-to-point wireless power transfer systems, recent work has considered wireless power transfer in the context of multiple-input single-output (MISO) distributed transmission systems [5]. The idea is to leverage principles of distributed transmit beamforming (DTB) developed for wireless communication systems [6]–[9] to improve the efficiency WPT systems. Specifically, we consider a transmit beamforming scenario in which two or more *separate* transmitters control the phase of their passband transmissions so that the signals constructively combine at the intended receiver. For a transmit cluster with M nodes and per-node power constraints, fully-coherent distributed transmit beamforming results in an M^2 power gain on target with respect to single-node transmission and a factor of M power gain on target with respect to non-coherent transmission [10], [11].

The setting considered in this paper and in [5] is illustrated in Fig. 1. We assume a system with M transmit nodes and one receive node. Each node in the system is further assumed to possess an independent local oscillator and a single isotropic antenna. No exogenous synchronization signals are available to the transmit nodes, hence the local oscillators

experience stochastic dynamics and the passband signals from each transmitter experience phase and frequency drift over time. The receive node periodically estimates the phases of the forward link channels during short measurement epochs and provides feedback on the reverse link to facilitate coherent transmission and passband signal alignment in the forward link and mitigate the effect of the independent oscillators at the transmit nodes. The receive node is also equipped with energy harvesting and storage devices which can harvest and store the energy received via WPT on the forward link for future utilization.

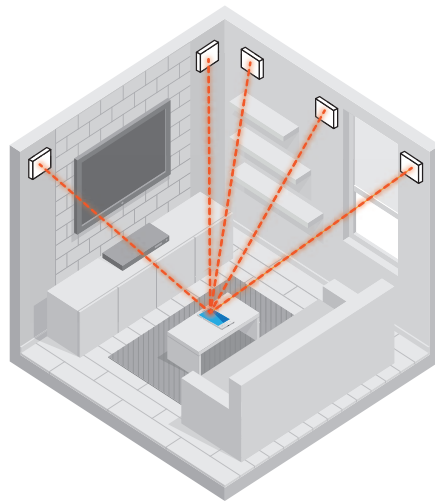


Fig. 1. System model example with $M=5$ transmit nodes.

Since periodic feedback improves the beamforming gain but requires the receivers to expend energy, there is a *fundamental tradeoff* between the feedback period and the efficiency of the WPT system. One strategy is for the receive nodes to provide no feedback. In this case, the transmit nodes can not correct for their channel phases or oscillator dynamics and the receive nodes can only harvest incoherent power (on average). Another strategy is for the receive nodes to provide extremely frequent feedback. In this case, even if the transmit nodes are able to form a perfectly coherent beam to the receiver, the energy cost of the feedback may exceed the actual harvested energy and the net harvested energy may be negative. Intuitively, there should be an optimal feedback period such that the receivers

can maximize their mean energy harvesting rate.

The prior work in [5] analyzed the optimum feedback rate under two simplifying assumptions: a simple one-state model for the stochastic oscillator dynamics and a simple receive node energy consumption model. This paper extends and generalizes [5] by analyzing the optimum feedback rate under a more accurate two-state model [12] for the stochastic oscillator dynamics and a more accurate receive node energy consumption model [13] to account for RF amplifier and the transmission circuitry power. The two-state model incorporates random walk frequency noise to better characterize long-term instabilities in the local oscillators and generally results in significantly higher optimum feedback rates than reported in [5]. A difficulty caused by the two-state model, however, is that the optimum feedback rate must be computed numerically. We develop an efficient search strategy by bounding the feasible region of the optimization problem. Numerical results are also provided to demonstrate that the efficiency of wireless power transfer can be significantly improved with feedback-based distributed transmit beamforming and feedback rate optimization.

II. SYSTEM MODEL

We assume the feedback-based (also called “receiver-coordinated”) protocol as described in [5], [8]. Forward link transmissions are divided into measurement and beamforming epochs, repeating periodically with period T_f . The time duration for measurement and beamforming epochs are T_m and $T_f - T_m$, respectively. During the measurement epoch, the receiver measures the forward link channels for subsequent feedback to facilitate distributed coherent transmission. During the beamforming epoch, the transmit nodes use the feedback to calculate an appropriate beamforming vector for distributed coherent transmission to the receiver.

During the measurement epoch, each transmit node separately transmits a short sounding signal to facilitate channel phase estimation at the receive node. Hence, the duration of the measurement epoch T_m is proportional to the number of transmit nodes, i.e., $T_m = MT_0$, where T_0 is a fixed measurement duration for a single transmit node.

Assuming identical forward link channel gains of g and transmitting power per node of P_0 , the mean beamforming power at any prediction time t in a steady-state beamforming epoch can be expressed as [8]

$$\bar{J}(T_f, t) = g^2 P_0 \left(M^2 e^{-\sigma_\phi^2(T_f, t)} + M \left(1 - e^{-\sigma_\phi^2(T_f, t)} \right) \right) \quad (1)$$

where $\sigma_\phi^2(T_f, t)$ is the steady-state variance of the phase prediction at time t after a measurement epoch for a given a frame period T_f . Observe that, for $\sigma_\phi^2(T_f, t)$ small, the mean beamforming power $\bar{J}(T_f, t) \approx g^2 P_0 M^2$. For $\sigma_\phi^2(T_f, t)$ large, $\bar{J}(T_f, t) \approx g^2 P_0 M$. The former case corresponds to ideal coherent beamforming and the latter case corresponds to incoherent transmission.

Intuitively, when T_f is large, $\sigma_\phi^2(T_f, t)$ is typically large and the receive node can only harvest non-coherent power. As T_f

decreases, $\sigma_\phi^2(T_f, t)$ is typically smaller and the receive node can harvest increased power due to coherency. This comes at a cost, however, due to the energy required to provide more frequent feedback to the transmit cluster. To analyze this tradeoff, the following section describes the tracking model used to characterize $\sigma_\phi^2(T_f, t)$.

III. TRACKING MODEL

Adopting the convention that the receive node is node 0, we define the discrete-time state of the i^{th} node’s carrier as $\mathbf{x}_i[k] := [\phi_i[k], \omega_i[k]]^T$, where $\phi_i[k]$ and $\omega_i[k]$ corresponds to the carrier phase and frequency offsets in radians and radians per second at node $i \in \{0, \dots, M\}$. The state update of the i^{th} node’s carrier is then $\mathbf{x}_i[k+1] = \mathbf{F}(T)\mathbf{x}_i[k] + \mathbf{u}_i[k]$ with

$$\mathbf{F}[T] = \begin{bmatrix} 1 & T \\ 0 & 1 \end{bmatrix}$$

where T is an arbitrary sampling period selected to be small enough to avoid phase aliasing at the largest expected frequency offsets. The process noise vector $\mathbf{u}^{(i)}$ i.i.d. $\mathcal{N}(\mathbf{0}, \mathbf{Q}_i(T))$ causes the carrier derived from the local oscillator at the transmit node to deviate from an ideal linear phase trajectory. The covariance of the discrete-time process noise is derived from a continuous-time model in [12] as

$$\mathbf{Q}_i(T) = \omega_F^2 T \begin{bmatrix} p_i + q_i \frac{T^2}{3} & q_i \frac{T}{2} \\ q_i \frac{T}{2} & q_i \end{bmatrix} \quad (2)$$

where ω_F is the forward link common carrier frequency in radians per second and p_i (units of seconds) and q_i (units of Hertz) are the process noise parameters corresponding to white frequency noise and random walk frequency noise, respectively, at node i . We assume that all of the oscillators have the same process noise parameters, i.e., $p_i \equiv p$ and $q_i \equiv q$ for all $i \in \{0, \dots, M\}$ for the remainder of the paper.

We denote the phase of the i^{th} forward link propagation channel as ψ_i and assume this quantity to be time invariant. The *pairwise offset* between the i^{th} transmit node and the receive node after propagation is defined as

$$\delta_i[k] = \mathbf{x}_i[k] + \begin{bmatrix} \psi_i \\ 0 \end{bmatrix} - \mathbf{x}_0[k]. \quad (3)$$

Therefore, the state update equation can be written as

$$\begin{aligned} \delta_i[k+1] &= \mathbf{F}(T)\delta_i[k] + \mathbf{u}_i[k] - \mathbf{u}_0[k] \\ &= \mathbf{F}(T)\delta_i[k] + \mathbf{G}\mathbf{w}_i[k] \end{aligned} \quad (4)$$

where

$$\mathbf{G} = \begin{bmatrix} 1 & 0 & -1 & 0 \\ 0 & 1 & 0 & -1 \end{bmatrix} \text{ and } \mathbf{w}_i[k] = \begin{bmatrix} \mathbf{u}_i[k] \\ \mathbf{u}_0[k] \end{bmatrix}. \quad (5)$$

Assuming the observations to be short such that the receiver can only measure the phase offset, the observation of the i^{th} forward link channel at the receiver is then

$$y_i[k] = \mathbf{h}\delta_i[k] + v_i[k] \quad (6)$$

where $\mathbf{h} = [1, 0]$ and $v_i[k]$ i.i.d. $\mathcal{N}(0, R)$ is the measurement noise which is assumed to be spatially and temporally i.i.d..

We assume the pairwise offset states are tracked individually, i.e., using M separate two-state Kalman filters. It can be shown that the system described in (4) and (6) is completely observable and completely controllable, hence the Kalman filter steady-state prediction covariance $\mathbf{P}(T_f) \in \mathbb{R}^{2 \times 2}$ is the unique positive definite solution of the discrete-time algebraic Riccati equation (DARE) [14]

$$\mathbf{P}(T_f) = \mathbf{F}(T_f) \left[\mathbf{P}(T_f) - \frac{\mathbf{P}(T_f) \mathbf{h}^T \mathbf{h} \mathbf{P}(T_f)}{\mathbf{h} \mathbf{P}(T_f) \mathbf{h}^T + R} \right] \mathbf{F}^T(T_f) + \mathbf{Q}(T_f) \quad (7)$$

where

$$\mathbf{Q}(t) = \mathbf{G} \text{cov} \{ \mathbf{w}_i[k] \} \mathbf{G}^T = \begin{bmatrix} At + \frac{B}{3} t^3 & \frac{B}{2} t^2 \\ \frac{B}{2} t^2 & Bt \end{bmatrix} \quad (8)$$

with $A = 2\omega_F^2 p$ and $B = 2\omega_F^2 q$. Note that $\mathbf{P}(T_f) \succ \mathbf{0}$ corresponds to the covariance matrix of the steady-state Kalman filter predictions just prior to a measurement/observation. The Kalman filter steady-state estimation covariance immediately after receiving an observation can be expressed as

$$\mathbf{S}(T_f) = \mathbf{P}(T_f) - \frac{\mathbf{P}(T_f) \mathbf{h}^T \mathbf{h} \mathbf{P}(T_f)}{\mathbf{h} \mathbf{P}(T_f) \mathbf{h}^T + R}. \quad (9)$$

We denote $\hat{\mathbf{S}}(T_f, t) = \mathbf{F}(t) \mathbf{S}(T_f) \mathbf{F}^T(t)$ and note that the steady-state prediction covariance at any prediction time $t > 0$ after an observation can be written as $\hat{\mathbf{P}}(T_f, t) = \hat{\mathbf{S}}(T_f, t) + \mathbf{Q}(t)$. The steady-state phase prediction variance is then

$$\sigma_\phi^2(T_f, t) = \hat{P}_1(T_f, t) = \hat{S}_1(T_f, t) + Q_1(t). \quad (10)$$

where $\hat{P}_1(T_f, t)$, $\hat{S}_1(T_f, t)$, and $Q_1(t)$ denote the (1,1) elements of $\hat{\mathbf{P}}(T_f, t)$, $\hat{\mathbf{S}}(T_f, t)$, and $\mathbf{Q}(t)$, respectively.

IV. ANALYSIS

In this section, we provide a method to calculate the feedback period T_f to maximize the mean energy harvesting rate (MEHR) at the receiver under steady-state tracking. The MEHR is defined as

$$\text{MEHR} = \frac{E_h}{T_f} = \frac{E_b - E_r}{T_f} \quad (11)$$

where E_b is the total average forward link beamforming energy and E_r is the reverse link feedback energy. The total average beamforming energy obtained by the receive node during a steady-state period of the protocol is

$$E_b = \eta \int_{t=T_m}^{T_f - T_m} \bar{J}(T_f, t) dt \quad (12)$$

where $\eta \in (0, 1)$ is the energy harvesting efficiency. According to [13], the energy consumption can be modeled as

$$E_r = \left[\frac{\zeta}{\mu} P_t + P_c \right] T_{on} + P_{tr} T_{tr} \quad (13)$$

where μ is the drain efficiency of the RF amplifier, ζ is the Peak to Average Ratio, P_t is the power for feedback transmission, P_c and P_{tr} are the power consumptions of the

transmitter circuitry on active and transient mode, respectively, and T_{on} and T_{tr} are the durations of the transmitter circuitry on active and transient mode, respectively. Our goal is to find the optimal feedback period $T_f^* > T_m$ to maximize (11).

A. Bounding the Feasible Region

In this section, we develop an efficient method to bound the feasible region for the MEHR maximization Problem into a closed interval. For notational convenience, we will analyze the normalized MEHR, defined as

$$\text{NMEHR} = \frac{\text{MEHR}}{\eta g^2 P_0 M}. \quad (14)$$

Since we are interested in frame periods that result in energy harvesting rates that exceed incoherent energy harvesting, we can define the set

$$\mathcal{X}_{\text{NMEHR}} = \{ T_f \geq T_m : \text{NMEHR} \geq 1 \}. \quad (15)$$

To facilitate analysis, we consider a function $\Phi(T_f)$ which is an upper bound for the NMEHR for all $T_f \geq T_m$. Hence, the set $\mathcal{X}_\Phi = \{ T_f \geq T_m : \Phi(T_f) \geq 1 \}$ is a superset of $\mathcal{X}_{\text{NMEHR}}$, i.e., $\mathcal{X}_{\text{NMEHR}} \subseteq \mathcal{X}_\Phi$. If $\mathcal{X}_{\text{NMEHR}}$ is nonempty, then it and \mathcal{X}_Φ must contain the value of T_f resulting in the globally optimal NMEHR, which is the solution of the MEHR maximization problem. Conversely, if \mathcal{X}_Φ is empty, then $\mathcal{X}_{\text{NMEHR}}$ is also empty and the optimal strategy is to set $T_f = \infty$ to simply harvest incoherent energy without feedback. The result is summarized in Proposition 1.

Proposition 1. Define

$$\hat{S}_1^{(0)}(T_f, t) = t^2 \sqrt{AB + \frac{B^2}{12} T_f^2}, \text{ and} \quad (16)$$

$$D = \frac{1}{M-1} \left(T_m + \frac{E_r}{\eta g^2 P_0 M} \right) > 0, \text{ and} \quad (17)$$

$$\beta = \sqrt{\int_0^\infty e^{-2Q_1(t)} dt} > 0 \quad (18)$$

where $Q_1(t)$ is the (1,1) element of the process noise covariance matrix $\mathbf{Q}(t)$. For all $T_f \geq T_m$, we have

$$\Phi(T_f) = 1 + \frac{M-1}{T_f} (\beta \Lambda(T_f) - D) \geq \text{NMEHR} \quad (19)$$

with

$$\Lambda(T_f) = \frac{1}{\left(\frac{8}{\pi} \hat{S}_1^{(0)}(T_f, 1) \right)^{\frac{1}{4}}} \quad (20)$$

This result implies that \mathcal{X}_Φ is either an empty set or a closed bounded interval $[T_m, T_{ub}]$, where T_{ub} is the solution to

$$\Lambda(T_{ub}) = \frac{D}{\beta}. \quad (21)$$

Due to the monotonicity of Λ , T_{ub} can be found easily using a simple bisection search method. If no value of $T_{ub} > T_m$ is found, then the optimal strategy is to provide no feedback and to simply harvest incoherent energy. In the following section, we assume $T_{ub} > T_m$ such that $\mathcal{X}_\Phi = [T_m, T_{ub}] \neq \emptyset$ is a bounded interval and develop a method to search the maximum NMEHR over \mathcal{X}_Φ .

B. Maximizing the MEHR on the Bounded Search Region

Based on the analysis in the prior section, we assume in this section that we have a closed bounded nonempty interval $\mathcal{X}_\Phi = [T_m, T_{ub}]$ for the feasible region of the MEHR maximization problem. One approach to solving one-dimensional optimization problems like the MEHR maximization problem is to use the DIRECT algorithm [15]. The DIRECT optimization algorithm solves a class of *global* optimization problems over closed bounded intervals. Application of the DIRECT algorithm requires (i) a bounded search region and (ii) the objective function is continuous or at least continuous in the neighborhood of a global optimum [15]. In Section IV-A, we bounded the search region of the optimal frame period by \mathcal{X}_Φ . The following proposition establishes that the NMEHR is a continuous function of T_f on the domain $[T_m, \infty)$ and thus, on $\mathcal{X}_\Phi \subseteq [T_m, \infty)$.

Proposition 2. *The NMEHR defined in (14) is a continuous function with respect to the feedback period T_f on the domain $[T_m, \infty)$.*

In light of Proposition 2, we can apply the DIRECT algorithm straightforwardly on the closed bounded domain \mathcal{X}_Φ . The following section presents numerical results based on the MEHR-maximizing search strategies developed in this section. The results show that the optimal frame period can be found successfully and efficiently using the proposed algorithms.

V. NUMERICAL RESULTS

This section provides numerical results to demonstrate the potential for distributed transmit beamforming for wireless power transfer. Table I lists the parameters of the oscillators and other general parameters for both forward and reverse links, where OSS and OLS denote ‘‘oscillator short-term stability’’ and ‘‘oscillator long-term stability’’ parameters, respectively. The process noise parameters p and q in Table I are chosen based on typical inexpensive crystal oscillator parameters [16] and Rakon RFPO45 oven-controlled oscillator datasheet [17]. Table II and Table III list the particular parameters for forward and reverse links, respectively. The power consumption of transmitter circuitry P_c is calculated according to paper [13], which includes the power consumption of the mixer, the frequency synthesizer, the digital-to-analog converter and the filters.

Using a link-budget analysis as in [5], the minimum transmit power for the receive node sending feedback is $-101 + 60.07 + 30 \log_{10}(d) - G_r = -19.96$ dBm or 1.01×10^{-5} Watts. We assume the transmit power for the receive node sending feedback is $P_t = 2 \times 10^{-5}$ Watts. The time to send feedback to one transmit node is $\frac{L}{R_R} = 5.33 \times 10^{-6}$ sec. Hence, the total time to send feedback to all transmit nodes, which is also the duration of the transmitter circuitry on active mode, is $T_{on} = M \cdot 5.33 \times 10^{-6}$ sec. Based on (13), the total feedback energy of $E_r = (M \cdot 5.33 + 2.50) \times 10^{-7}$ Joules.

Figure 2 shows the optimal feedback rate (in Hertz) and the maximum NMEHR versus oscillator parameters p and q for

TABLE I
GENERAL PARAMETERS.

| Case | Parameter | Value | Units | Meaning |
|-----------------|-----------|------------------------|-------|------------------------------|
| good XO | p | 2.48×10^{-24} | sec | OSS |
| | q | 7.44×10^{-27} | Hertz | OLS |
| poor XO | p | 6.34×10^{-18} | sec | OSS |
| | q | 2.57×10^{-23} | Hertz | OLS |
| Rakon RPFO45 | p | 2.31×10^{-21} | sec | OSS |
| | q | 6.80×10^{-23} | Hertz | OLS |
| | d | 5 | meter | link distance |
| | α | 3 | | path loss exponent |
| | η | 0.70 | | energy harvesting efficiency |

TABLE II
PARAMETERS FOR FORWARD LINK.

| Parameter | Value | Units | Meaning |
|------------|---------------------|------------------|--|
| ω_F | $2\pi \times 10^9$ | rad/sec | forward link carrier frequency |
| T_0 | 50×10^{-6} | sec | duration of measurement for single transmit node |
| P_0 | 1 | Watts | transmit power for single transmit node |
| L | 32 | | number of bits per channel measurement |
| G_t | 6 | dBi | transmit node’s antenna gains |
| R | 5×10^{-10} | rad ² | measurement noise |

small network ($M = 2$) and large network ($M = 100$), respectively. It is observed that the optimal feedback rate increases when either oscillator parameter p or oscillator parameter q increases. Since in order to achieve the maximum NWMEHR, the system requires the channel information more frequently to compensate for the bad channel estimation caused by the poor oscillator parameters. In all four subplots, we also show dark blue regions in where no feedback is needed. In these areas, the system has low-quality oscillators and thus, the increment of the beamforming power by increasing the feedback rate can not compensate for the increment of the energy for feedback.

Figure 3 shows the optimal feedback rate (in Hertz) and

TABLE III
PARAMETERS FOR REVERSE LINK.

| Parameter | Value | Units | Meaning |
|------------|----------------------|---------|-----------------------------------|
| ω_R | $4.8\pi \times 10^9$ | rad/sec | reverse link carrier frequency |
| B_R | 10×10^6 | Hertz | reverse link bandwidth |
| R_R | 6 | Mbps | reverse link data rate |
| G_r | 0 | dBi | receive node’s antenna gains |
| P_c | 0.1 | Watts | circuitry power on active mode |
| P_{tr} | 0.05 | Watts | circuitry power on transient mode |
| T_{tr} | 5×10^{-6} | sec | duration on transient mode |
| ζ | 10 | dB | Peak to Average Ratio |
| μ | 0.35 | | drain efficiency of RF amplifier |

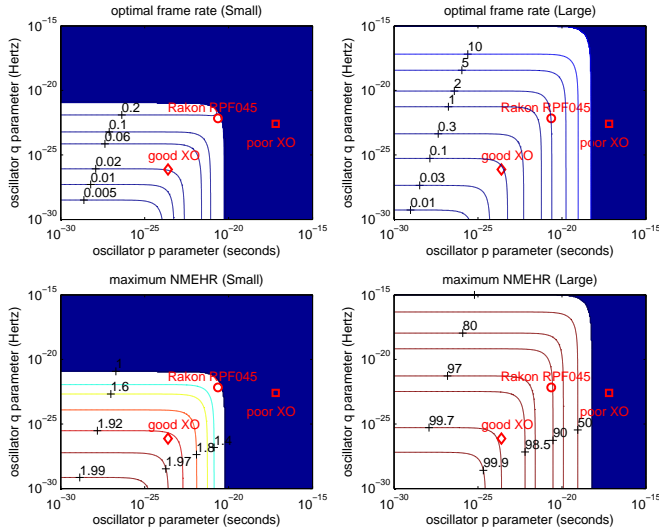


Fig. 2. Optimal feedback rate (in Hertz) and maximum NMEHR versus oscillator parameters p and q for small network ($M = 2$) and large network ($M = 100$). The shaded region corresponds to conditions under which the optimal strategy is to set the optimal feedback rate to zero and harvest incoherent energy.

maximum MEHR (in milliwatts) versus number of transmit nodes. We can observe that the optimal feedback rate increases with the number of transmit nodes M . This is caused by the fact that the feedback energy is linear with M and the system needs more frequent feedback to compensate for the feedback energy consumption. These results also show, as expected, the maximum MEHR always lies between the coherent power level and the incoherent power level. The maximum MEHR gradually deviates from the fully coherent beamforming power to the incoherent beamforming power with increasing number of transmit nodes.

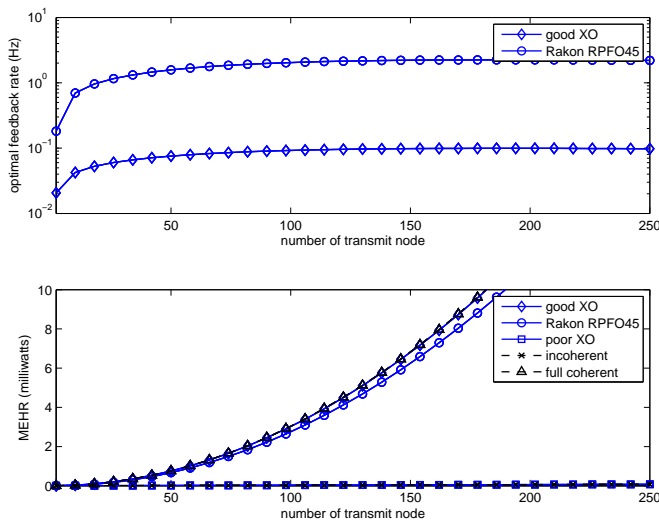


Fig. 3. Optimal feedback rate (in Hertz) and maximum MEHR (in milliwatts) versus number of transmit nodes.

VI. CONCLUSION

This paper considers the combination of feedback-based distributed transmit beamforming and wireless power transfer. The analysis includes a two-state dynamic model for the oscillator dynamics and a realistic model for receive-node energy consumption. A method for finding the optimal feedback rate to maximize the mean energy harvesting rate is presented. Numerical results demonstrate the method and show that distributed beamforming can improve the efficiency of wireless power transfer and energy harvesting.

REFERENCES

- [1] V. Liu, A. Parks, V. Talla, S. Gollakota, D. Wetherall, and J. R. Smith, "Ambient backscatter: Wireless communication out of thin air," in *Proceedings of the ACM SIGCOMM 2013 Conference on SIGCOMM*, 2013, pp. 39–50.
- [2] J. R. Smith, *Wirelessly Powered Sensor Networks and Computational RFID*. Springer, 2013.
- [3] L. Varshney, "Transporting information and energy simultaneously," in *Information Theory, 2008. ISIT 2008. IEEE International Symposium on*, July 2008, pp. 1612–1616.
- [4] L. Liu, R. Zhang, and K.-C. Chua, "Wireless information and power transfer: A dynamic power splitting approach," *Communications, IEEE Transactions on*, vol. 61, no. 9, pp. 3990–4001, September 2013.
- [5] R. Wang and D.R. Brown III, "Feedback rate optimization in receiver-coordinated distributed transmit beamforming for wireless power transfer," in *Information Sciences and Systems (CISS), 2015 49th Annual Conference on*, March 2015.
- [6] R. Mudumbai, D. Brown, U. Madhow, and H. Poor, "Distributed transmit beamforming: challenges and recent progress," *Communications Magazine, IEEE*, vol. 47, no. 2, pp. 102–110, February 2009.
- [7] R. Preuss and D.R. Brown III, "Two-way synchronization for coordinated multicell retrodirective downlink beamforming," *Signal Processing, IEEE Transactions on*, vol. 59, no. 11, pp. 5415–5427, Nov 2011.
- [8] D.R. Brown III, P. Bidigare, and U. Madhow, "Receiver-coordinated distributed transmit beamforming with kinematic tracking," in *Acoustics, Speech and Signal Processing (ICASSP), 2012 IEEE International Conference on*, March 2012, pp. 5209–5212.
- [9] D.R. Brown III and R. David, "Receiver-coordinated distributed transmit nullforming with local and unified tracking," in *Acoustics, Speech and Signal Processing (ICASSP), 2014 IEEE International Conference on*, May 2014, pp. 1160–1164.
- [10] P. Bidigare, M. Oyarzun, D. Raeman, D. Cousins, D. Chang, R. O'Donnell, and D.R. Brown III, "Implementation and demonstration of receiver-coordinated distributed transmit beamforming across an ad-hoc radio network," in *Proc. of the 46th Asilomar Conf. on Signals, Systems, and Computers*, Pacific Grove, CA, November 4-7 2012, pp. 222–226.
- [11] D. Scherber, R. O'Donnell, M. Rebholz, M. Oyarzun, C. Obranovich, W. Kulp, P. Bidigare, and D.R. Brown III, "Coherent distributed techniques for tactical radio networks: Enabling long range communications with reduced size, weight, power and cost," in *MILCOM 2013*, San Diego, CA, November 18-20 2013.
- [12] L. Galleani, "A tutorial on the 2-state model of the atomic clock noise," *Metrologia*, vol. 45, no. 6, pp. S175–S182, Dec. 2008.
- [13] S. Cui, A. Goldsmith, and A. Bahai, "Energy-constrained modulation optimization," *Wireless Communications, IEEE Transactions on*, vol. 4, no. 5, pp. 2349–2360, Sept 2005.
- [14] Y. Bar-Shalom, X. Rong Li, and T. Kirubarajan, *Estimation with Applications to Tracking and Navigation*. John Wiley and Sons, 2001.
- [15] D. R. Jones, C. D. Pertunnen, and B. E. Stuckman, "Lipschitzian optimization without the lipschitz constant," *J. Optim. Theory Appl.*, vol. 79, no. 1, pp. 157–181, Oct. 1993.
- [16] W. Klepczynski and P. Ward, "Frequency stability requirements for narrow band receivers," in *32nd Annual Precise Time and Time Interval Meeting*, November 2000.
- [17] "Rakon RFPO45 crystal oscillator datasheet," 2009. [Online]. Available: <http://www.rakon.com/Products/Public/Documents/Specifications/RFPO45.pdf>